Optimal Sensing Protocol for Statistically Polarized Nano-NMR with NV Centers

Nicolas Staudenmaier[1,*], Anjusha Vijayakumar-Sreeja,[1,*] Genko Genov[1,*], Daniel Cohen[2]
Christoph Findler[1,3], Johannes Lang,[1,3] Alex Retzker,[2,4] Fedor Jelezko,[1] and Santiago Oviedo-Casado[2,5,†]

[1]*Institute for Quantum Optics, Ulm University, Albert-Einstein-Allee 11, 89081 Ulm, Germany*
[2]*Racah Institute of Physics, Hebrew University of Jerusalem, 91904 Jerusalem, Israel*
[3]*Diatope GmbH, Buchenweg 23, 88444 Ummendorf, Germany*
[4]*AWS Center for Quantum Computing, Pasadena 91125, California, USA*
[5]*Área de Física Aplicada, Universidad Politécnica de Cartagena, Cartagena E-30202, Spain*

Diffusion noise represents a major constraint to successful liquid state nano-NMR spectroscopy. Using the Fisher information as a faithful measure, we theoretically calculate and experimentally show that phase sensitive protocols are superior in most experimental scenarios, as they maximize information extraction from correlations in the sample. We derive the optimal experimental parameters for quantum heterodyne detection (Qdyne) and present the most accurate statistically polarized nano-NMR Qdyne detection experiments to date, leading the way to resolve chemical shifts and J couplings at the nanoscale.

Phase sensitive protocols, such as quantum heterodyne detection (Qdyne), optimize the precision of frequency estimation from classical signals in noisy environments by sequentially sampling the probe at periodic intervals, thereby overcoming the limited coherence time of the quantum sensor [1–3]. Then, resolving arbitrarily close frequencies should be possible by increasing the total measurement time [4,5]. These results heralded the possibility of performing effective nuclear magnetic resonance at the nanoscale (nano-NMR), on statistically polarized liquid samples, with quantum probes; for example, single nitrogen-vacancy (NV) centers in diamond [6–10]. However, despite the early promising results, these protocols have been scarcely applied in experiments with chemically or pharmacologically relevant samples [3,11–16]. The foremost difficulty explaining this reluctance is the necessary trade-off between sensor-sample interaction strength and short diffusion time, typical of statistically polarized samples. This combines with a seemingly challenging data acquisition and postprocessing, and the existence of more amenable alternatives such as correlation spectroscopy (CS) [6,17].

The archetypal color defects used for single NV nano-NMR are located at depths d a few nm below the diamond surface, where they interact via dipole-dipole coupling with nuclei from a sample located on top of the diamond surface. With the interaction strength decreasing as $\sim d^{-3}$, only the closest nuclei contribute significantly to the total interaction. Then, for shallow NV centers, the statistical polarization of the nuclei is significant enough to overcome any thermal averaging [6,18–20]. These statistically polarized nuclei generate a time-correlated magnetic field $B(t) = \sum_i a_i(t)\cos(\omega_i t) + b_i(t)\sin(\omega_i t)$, that can contain

oscillations at several (e.g., Larmor) frequencies ω_i. $B(t)$ generates a detectable change on the NV center electron spin state, thereby providing valuable information about the sample. However, as molecules diffuse, the couplings between nuclei and NV center—the amplitudes $\{a(t), b(t)\}$—fluctuate. This is typically modeled as a random process normally distributed around zero and with finite correlation time $T_D = d^2/D$, with D the diffusion coefficient of the fluid [21]. It is commonly accepted that, when the diffusion time T_D is shorter than an oscillation period of $B(t)$, one cannot accumulate enough information per measurement to resolve the respective spectral line. Yet recently, it was demonstrated that correlations between diffusing nuclei survive longer than T_D, allowing us to significantly extend the data acquisition time and, consequently, the precision of estimation of the target frequency [22–25].

In this Letter, we determine the optimal experimental parameters for two state-of-the-art quantum sensing protocols, aiming to get the maximum information for spectral reconstruction. We combine this strong theoretical foundation with robust data analysis, allowing us to present the most accurate statistically polarized nano-NMR Qdyne experiments to date. We compare them to ideal, error-free CS experiments through the amount of information that they provide about a target signal frequency, and unambiguously establish that Qdyne has a superior performance. These results open new possibilities for high precision quantum sensing, broadening the scope for implementing Qdyne in liquid nano-NMR, conceivably allowing us to resolve chemical shifts and J coupling at the nanoscale. Additionally, we demonstrate a universal comparison methodology for sensing protocols and experimental

platforms that can potentially become a valuable tool for optimizing any quantum sensing experiment.

Quantifying information.—We consider an NV center interacting with the magnetic field $B(t)$ generated by a statistically polarized sample of diffusing nuclei. Assuming that any other external noise is strongly suppressed by either dynamical decoupling (DD) [26–32] or careful experimental design, the main limiting factor to spectral resolution is the finite correlation time, T_D, of $B(t)$. An initial superposition state of the NV center interacting with $B(t)$, accumulates a phase $\Phi[B(t)]$. Tracking the evolution of such state permits inferring the parameters describing $B(t)$ using suitable postprocessing.

Experimentally, the mean squared error (MSE) $\Delta\delta$ quantifies the accuracy in estimating a parameter; e.g., the small (angular) frequency offset δ, defined as the difference between the nuclear spin Larmor frequency and the sampling frequency [33]. The Cramér-Rao bound states that the MSE must always be greater than the inverse Fisher information about the parameter, $\Delta\delta \geq 1/I_\delta$ [43,44], establishing a connection between theory and experiments, and providing a direct route to improve experiments through theoretical modeling. For a single measurement

$$i_\delta = \mathbb{E}\left[\left(\frac{d\log[L(\delta)]}{d\delta}\right)^2\right], \qquad (1)$$

with $L(\delta)$ the likelihood of finding the NV in a given state. After N measurements in an experiment of duration T, the total information is $I_\delta = \sum_N i_\delta$. We aim to theoretically maximize I_δ for a given protocol, seeking the best possible experimental $\Delta\delta$.

Here, we compare Qdyne with one of the most advanced sensing protocols: correlation spectroscopy [6,17]. We benchmark the achievable I_δ for each protocol, in the scenario of a magnetic signal with a limited coherence time originating from a statistically polarized sample, by defining the ratio

$$R_\delta = I_\delta^{\text{Qdyne}}/I_\delta^{\text{CS}}, \qquad (2)$$

between the Fisher information of Qdyne I_δ^{Qdyne} and CS I_δ^{CS}. In what follows, we theoretically calculate I_δ for each protocol showing that, in most experimental scenarios, $R_\delta > 1$. Then, we compare it to $\Delta\delta$ obtained from statistically polarized nano-NMR experiments and demonstrate strong accord with the theoretical modeling.

Correlation spectroscopy.—Standard quantum spectroscopy with NV centers monitor their fluorescence response, which is modulated by the accumulated phase $\Phi[B(t)]$ in each measurement. Then, one infers information about $B(t)$ by averaging the results of all measurements. Since $B(t)$ is time correlated, consecutive phase acquisition periods are also correlated, and encode information about $B(t)$. CS builds upon this notion by combining two phase acquisition
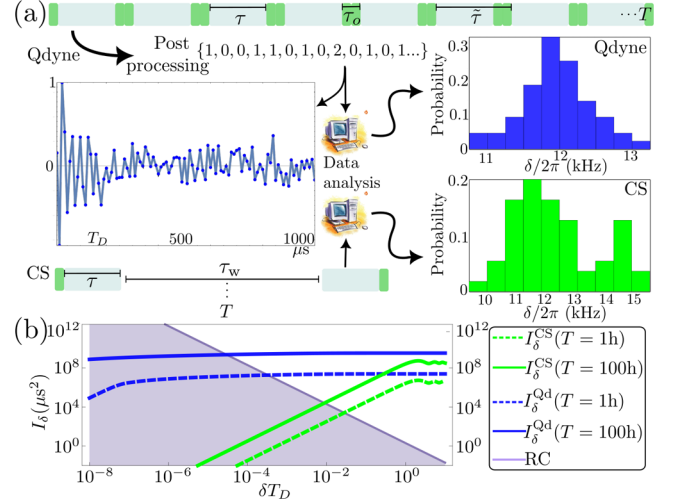
FIG. 1. (a) Depiction of Qdyne (Qd, upper part) and correlation spectroscopy (CS, lower part) experimental procedures for NV-NMR on a fluid sample with diffusion time T_D. For Qdyne, the measurement sequence is repeated at fixed time intervals $\tilde{\tau}$. During each overhead time τ_o the NV is interrogated about the phase acquired during the time τ and repolarized for a new measurement. The recorded photons are postselected to obtain a measurement vector whose autocorrelation resembles the covariance of the noise model. In CS, the autocorrelation of the sample is probed directly by changing the waiting τ_w between two DD blocks. Data analysis using maximum likelihood estimation produces a histogram of estimators which, for low frequencies, is narrower for Qdyne than for CS. (b) Exact Fisher information I_δ for both CS [Eq. (3)] and Qdyne [Eq. (4)] with total measurement time $T = 1$ hour and $T = 100$ hours. The shadowed area marks the frequencies for which the information is insufficient for successful estimation, set at $\Delta\delta < \delta^2/4$, as per the Rayleigh criterion (RC). For all I_δ $\Phi_{\text{rms}} = 1$, with $T_D = 100$ μs, $\eta_0 = 0.04$, $\eta_1 = 0.03$, and for Qdyne $\tilde{\tau} = 25$ μs.

periods of equal duration τ separated by a waiting time τ_w [see Fig. 1(a)]. The phase accumulated during the first period, is stored as population difference (transferred to a "memory" qubit) during τ_w [17], imposing $\tau_w \lesssim T_1$ (T_m), the latter being the spin-lattice (memory qubit) relaxation time. Varying τ_w yields a signal that corresponds to the covariance of the noise affecting the probe, i.e., $\text{cov}\langle\Phi[B(t')]\Phi[B(t'+t)]\rangle = \Phi_{\text{rms}}^2\cos(\delta t)C(t/T_D)$, where $t = \tau + \tau_w$, $\Phi_{\text{rms}} \propto B_{\text{rms}}$ the root-mean-squared field of $B(t)$, and $C(t/T_D)$ is the envelope that describes the decay of correlations due to noise. For diffusion, $C(t/T_D \ll 1) \sim \exp(-6t/T_D)$ while $C(t/T_D \gg 1) \sim t^{-3/2}$ [22].

In each readout, the expected photon number is $p = \eta + c\langle\sin(\Phi_0)\sin(\Phi_t)\rangle/2$, with $\eta = (\eta_0 + \eta_1)/2$ the average photon number (η_0 and η_1 are the expected photon numbers for readout of NV spin states $|0\rangle$ and $|1\rangle$, respectively), and $c = \eta_0 - \eta_1$ the contrast. Averaging over realizations of $B(t)$ yields the relation between the expected photon number and the autocorrelation, $p = \eta + c\Phi_{\text{rms}}^2\cos(\delta t)C(t/T_D)/2$. Using Eq. (1) with p

we get $i_\delta^{\text{CS}} = [c^2/(4\eta + c^2)]\Phi_{\text{rms}}^4 t^2 \sin^2(\delta t) C^2(t/T_D)$. To calculate I_δ, we transform the measurements sum into an integral and take the low frequency limit $(\delta/2\pi) < 1/T_D$ [33]. Then

$$I_\delta^{\text{CS}} = TT_D \int_0^1 dt \, i_\delta^{\text{CS}}(t) \approx \frac{c^2 \Phi_{\text{rms}}^4 \delta^2 T_D^3 T}{4\eta + c^2}, \qquad (3)$$

where we assume $T_1(T_m) \gg T_D$ and ignore its effect. The relation between δ, T_D, and T defines the ability to estimate δ. If $(\delta/2\pi)T_D > 1$, a complete oscillation occurs before the signal is strongly suppressed, and estimating the frequency poses no problem. Conversely, for $(\delta/2\pi)T_D < 1$, $\lim_{\delta\to 0} I_\delta^{\text{CS}}(T) = 0$. This is illustrated in Fig. 1(b), where we calculate $I_\delta^{\text{CS}}(T)$ using the exact analytical formula, for two different total experiment times T, and compare it against the maximum MSE that allows for frequency estimation, defined, following the Rayleigh criterion for linewidth separation in optics, as $\Delta\delta < \delta^2/4$ [45–47]. We observe that I_δ vanishes with δ faster than it grows with T. Note that both the oscillations and the relative flatness appearing at $(\delta/2\pi)T_D \gtrsim 1$ result from using the exact I_δ^{CS} rather than the approximate expression Eq. (3).

Qdyne.—Phase sensitive measurements consist of (phase-dependent) signal accumulation periods τ followed by qubit interrogation and repolarization (for overhead time τ_o) for the next measurement, in a process repeated continuously with periodic separation time $\tilde{\tau} = \tau + \tau_o$, as shown in Fig. 1(a) (see, also, [33] for a detailed description of Qdyne implementation). Following each interrogation, the expected photon number is $p = \eta + c\langle\sin(\Phi_t)\rangle/2$. A sequence of such equally spaced measurements directly reflects the time evolution of $B(t)$. To better understand Qdyne, we use polar coordinates and write $B(t) = \Omega(t) \cos[\delta t + \varphi(t)]$, with $\Omega(t) = \sqrt{a(t)^2 + b(t)^2}$ and $\tan[\varphi(t)] = b(t)/a(t)$. Then, when $T_D \gg 1/\delta$, $\tilde{\tau} \ll T_D$ and $\varphi(t)$ remains coherent for a sufficiently large number of measurements, allowing us to perform maximum likelihood estimation (MLE) over a small parameter space. Increasing T permits resolving arbitrarily small frequencies [4].

When $T_D < 1/\delta$, $\varphi(t)$ changes faster than the oscillation period $2\pi/\delta$. Then, each new measurement requires estimating new parameters, and MLE becomes computationally intractable. In this scenario, the solution is to calculate the autocorrelation of the measured signal during postprocessing [see Fig. 1(a)]. This treatment reduces the parameter space by having a decaying signal similar to that of CS. Then, the signal parameters can be estimated through, e.g., least squares algorithms. The advantage of Qdyne is that, by measuring sequentially, any two points in a measurement vector are correlated, instead of having just pairwise correlation, as in CS. For the power-law signals occurring in nanoscale diffusion [22,25], this means that

much more information is contained in the Qdyne autocorrelation. The relevant probability is that of obtaining a pair of correlated photons between any two measurements $\langle p_0 p_{j\tilde{\tau}}\rangle$, j being an integer, yielding $i_\delta^{\text{Qdyne}} = [c^4/(4\eta + c^2)^2]\Phi_{\text{rms}}^4 t^2 \cos(\delta t) C^2(t/T_D)$. We obtain the total information by integrating over t, with an added factor accounting for all correlated pairs of measurements [33]. Using normalized time $z = t/T_D$ we get

$$I_\delta^{\text{Qdyne}} = \frac{T_D^4}{\tilde{\tau}^2} \int_0^{\frac{T}{T_D}} dz \, i_\delta^{\text{Qdyne}}\left(\frac{T}{T_D} - z\right) \approx \frac{c^4 \Phi_{\text{rms}}^4 T_D^3 T \log \delta T}{(4\eta + c^2)^2 \tilde{\tau}^2}, \qquad (4)$$

where we consider $(\delta/2\pi)T_D < 1$ and $(\delta/2\pi)T > 1$. Equation (4) shows that, with Qdyne, spectral resolution no longer depends on the relation between T_D and δ, but solely on T, as illustrated in Fig. 1. There, only when $(\delta/2\pi)T < 1$ does $I_\delta^{\text{Qdyne}} \to 0$.

Equation (4) has several implications: Qdyne requires a high number of measurements, and therefore, a small $\tau_o = \tilde{\tau} - \tau$, and two measurements per correlation (whereas CS requires one), which translates to an extra $[c^2/(4\eta + c^2)]$, penalizing Qdyne due to the typically low average number of photons detected per measurement. Conversely, a small $(\delta/2\pi)T_D$ favors Qdyne as compared to CS. Thus, increasing the measurement time T permits estimating much smaller frequencies. The information ratio, Eq. (2), in the limit $\delta/2\pi < 1/T_D$ reads

$$R_\delta = \frac{I_\delta^{\text{Qdyne}}}{I_\delta^{\text{CS}}} \approx \frac{c^2}{4\eta + c^2} \frac{\log(\delta T)}{\delta^2 \tilde{\tau}^2}. \qquad (5)$$

Next, we theoretically explore the dependence of R_δ on different parameters and compare it to experimental results.

Experimental results and data analysis.—To test our theoretical model, we perform nano-NMR measurements on statistically polarized samples with single shallow NV centers. For both protocols, we record the signal coming from hydrogen nuclei in an immersion oil (Fluka 10976) with a Larmor frequency ≈ 2 MHz (see Refs. [25,33] for further details).

Data postprocessing is important for successful nano-NMR, especially when $(\delta/2\pi)T_D < 1$. Minimizing estimation errors requires using efficient estimators such as MLE [48] that can saturate the Cramér-Rao bound. Contrary to that, the typically employed Fourier transform offers sufficient statistics for parameter estimation only for signals with well separated frequencies and high signal-to-noise ratio. Moreover, estimating frequencies from Fourier peaks is sub-optimal [49], explaining its failure in the challenging nano-NMR regimes, which feature highly fluctuating coupling parameters and for frequency splittings that are smaller than $1/T_D$.

Our goal is to optimize $\Delta\delta$ and compare it to the theoretical calculations of I_δ. To have the most faithful comparison, we need MLE. However, as noted above, Qdyne measurement vectors become computationally intractable for MLE when $(\delta/2\pi)T_D < 1$. Rather, we resort to fitting the autocorrelation of the data to $\Phi_{\rm rms}^2 \cos(\delta t)C(t/T_D)$ with parameters $\{\Phi_{\rm rms}, \delta, T_D\}$ using a simple nonlinear least squares algorithm, which is equivalent to MLE if the variables to be fitted have normally distributed errors [33,50], which we can assume. Estimating the MSE from a single fit to the autocorrelation can be misleading, especially in the hardly resolvable regime, due to outliers, a highly nonconcave parameter space, and because a good initial estimation of the MSE is required. Instead, we calculate the root MSE (rmse) from a distribution of frequency estimators, obtained by fitting smaller blocks of the data. These are calculated by slicing the measurement vector onto 15 minute ($\sim 10^7$ measurements) pieces and then combining them in groups of 20. Thus, we achieve a balance between reducing noise and minimizing statistical errors. We benchmark the acquired squared inverse of the rmse against I_δ. A demonstration of the difference in data analysis procedures is shown in Fig. 2(a), where we display the probability histogram of δ estimators, with rmse = 458 Hz, together with the Fourier transform of the autocorrelation of the entire measurement vector, with rmse = FWHM/2 = 602 Hz [49,51]. To the best of our knowledge, the former represents the most precise statistically polarized Qdyne result to date [1].

In correlation spectroscopy, each experiment yields a single autocorrelation of $\Phi[B(t)]$, which we fit with a nonlinear least squares algorithm. We evaluate the data 100 times to the model with random initial parameters and

take the best fit, in terms of R^2. The frequency estimator and its rmse are obtained from the parameter estimates from the best model.

To obtain R_δ, we calculate, for each experiment, the theoretical I_δ for the alternative measurement protocol using the same parameters as in the experiment. We resort to this procedure given the difficulty of performing identical experiments with both protocols. This procedure excludes possible error sources present in the experiments, which results in a R_δ biased toward the theoretical calculation, in which these same errors are excluded. This accounts, in part, for not saturating the Cramér-Rao bound [33].

Figures 2(b) and 2(c) show the experimental results for R_δ over a theoretical background calculated exactly from the integrals in Eqs. (3) and (4), fixing all the parameters but two. This poses a problem when showing together theory and experiment, as different experiments have more than two different parameters. We solve the issue by scaling the experimental results according to the fixed parameters chosen for the theory background. This does not alter the relation between protocols (the experimental R_δ still reflects the best protocol for these parameters), and permits showing the optimal parameter regions for each protocol while at the same time demonstrating correspondence between theory and experiments. In each figure, we display the obtained ratio with the corresponding experimental result as filled shapes in the parameter space, while empty shapes represent full theoretical expectation. There is a small deviation between the full theoretical expectation and the ratio between theory and experiment. The similarity between the deviations for CS and Qdyne experiments show that both experimental setups are subject to similar, not-accounted-for, errors [33]. This represents a strong
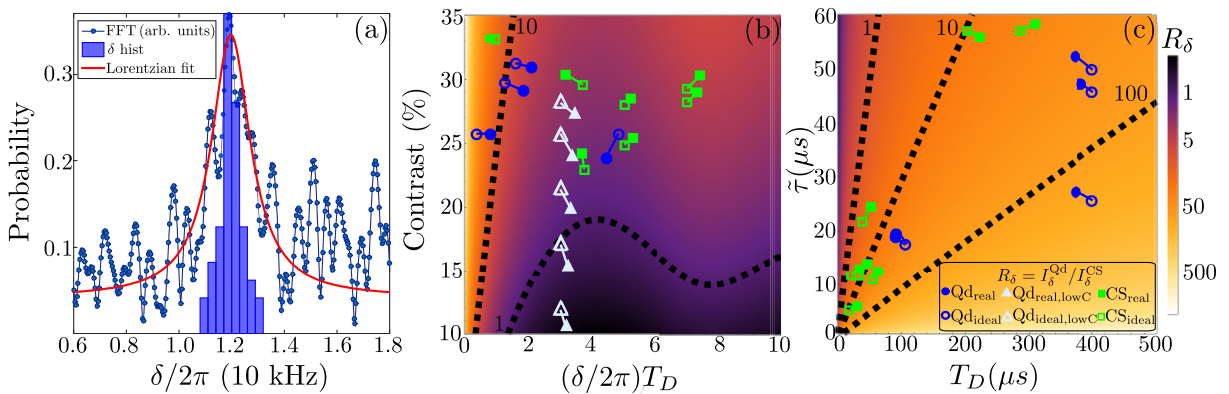
FIG. 2. Probability histogram of frequency estimators from several autocorrelation slices of a Qdyne (Qd) experiment and the Fourier transform of the full autocorrelation in (a). In (b) and (c), exact information ratio from Eq. (2) in logarithmic scale in the background. Ratio between the information obtained experimentally and the ideal information for the same parameters with the alternative protocol. Empty shapes represent the theoretical expectation for R_δ while full shapes show the experimental result. Thick dashed lines show reference R_δ. In (b), $T = 100$ hours, $\tilde{\tau} = 40$ μs, and $T_D = 50$ μs, while for (c) $(\delta/2\pi)T_D = 1$, with constant overhead time $\tau_o = 2.1$ μs [2]. Note that we use relative contrast defined as $(\eta_0 - \eta_1)/\eta_0$, for which purpose we scale Eqs. (3) and (4) appropriately, and we fix it to 25% ($\eta_0 = 0.04$, $\eta_1 = 0.03$) in (c). The legend and color bar in (c) apply to (b) as well.

validation of our theoretical modeling and shows that calculating I_δ is a mathematically consistent procedure for experimental optimization.

The main challenge for statistically polarized nano-NMR is to resolve spectral lines whose frequency difference is smaller than the inverse characteristic time $1/T_D$. In Fig. 2(b), we compare the performance of Qdyne and CS according to the relation between the target frequency and T_D. For small δ, the superior ability of Qdyne to capitalize on the long-lived power-law correlations means that it is the protocol of choice. Considering a reasonable $T = 100$ hours experiment, even at poor contrast, it proves superior to CS. A reduction in the total measurement time to $T = 1$ hour does not significantly change the theoretical superiority of Qdyne, as observed in Fig. 1(b). We note that long experimental times may be challenging for some biological applications. They can be further reduced by improving photon collection efficiency through engineering the diamond geometry [52–55], optimizing the sampled times [33], or through data postprocessing using machine learning [56]. When $(\delta/2\pi)T_D > 1$, the influence of the total measurement time diminishes, and the contrast gains importance, with CS preferred at poor contrast. However, typical experiments with single NV centers easily feature relative contrasts $> 20\%$ (rather, in excess of 30%), for which Qdyne performs better. To experimentally demonstrate that at low contrast $R_\delta < 1$, we have artificially altered the contrast during the postprocessing of the Qdyne data by choosing the photons from different lengths of the readout window [33] [triangles in Fig. 2(b)].

A crucial factor when setting up a nano-NMR experiment is that $\Phi_{\rm rms} \lesssim 1$ for optimal information acquisition [23,33]. But $\Phi_{\rm rms} \propto B_{\rm rms}\tau$, where the $B_{\rm rms}$ is given by the sample. Then, τ is relatively fixed by said condition [33]. For CS the effect is negligible, but for Qdyne, whose strategy is to measure at a fast rate to accumulate correlations, longer sequence times $\tilde{\tau}$ negatively affect $I_\delta^{\rm Qdyne}$ [note the $1/\tilde{\tau}^2$ factor in Eq. (4)]. In Fig. 2(c), we explore the influence of $\tilde{\tau}$ on the performance of Qdyne. For longer T_D, more information can be sampled with Qdyne than with CS, even for larger $\tilde{\tau}$. This is reflected by the lines of constant R_δ with approximately constant slope. Conversely, short diffusion times, resulting from very shallow NV centers, favor CS. But this is usually compensated by the shorter measurement times for NVs at low depth, resulting in Qdyne being superior for most of the parameter range. We note that the total information could be insufficient for parameter estimation for very low T_D, regardless of the protocol, as demonstrated in Fig. 1.

Conclusions.—Diffusion noise poses a major challenge for liquid nano-NMR, and requires refining the experimental design and data analysis for maximal information extraction. Here, we theoretically show and experimentally demonstrate that phase-sensitive, sequential measurements, such as Qdyne, combined with maximum likelihood estimation, can significantly enhance frequency estimation precision. We apply them in statistically polarized samples and compare with other advanced techniques such as correlation spectroscopy. We present a systematic procedure, based on the Fisher information, that allows us to both compare the protocols and optimize the sensing experiments. Our work is applicable to a wide variety of different platforms by changing the respective parameters to reflect the particulars of the experiment. Accordingly, we managed to perform the most accurate Qdyne experiments in liquid nano-NMR to date, providing a recipe toward executing efficient single NV nano-NMR with samples of biochemical importance and resolving chemical shifts or measuring J couplings.

---

*These authors contributed equally to this work.
†oviedo.cs@mail.huji.ac.il

[1] S. Schmitt, T. Gefen, F. M. Stürner, T. Unden, G. Wolff, C. Müller, J. Scheuer, B. Naydenov, M. Markham, S. Pezzagna, J. Meijer, I. Schwarz, M. Plenio, A. Retzker, L. P. McGuinness, and F. Jelezko, Submillihertz magnetic spectroscopy performed with a nanoscale quantum sensor, Science **356**, 832 (2017).

[2] J. M. Boss, K. S. Cujia, J. Zopes, and C. L. Degen, Quantum sensing with arbitrary frequency resolution, Science **356**, 837 (2017).

[3] D. R. Glenn, D. B. Bucher, J. Lee, M. D. Lukin, H. Park, and R. L. Walsworth, High-resolution magnetic resonance

spectroscopy using a solid-state spin sensor, Nature (London) **555,** 351 (2018).

[4] A. Rotem, T. Gefen, S. Oviedo-Casado, J. Prior, S. Schmitt, Y. Burak, L. McGuiness, F. Jelezko, and A. Retzker, Limits on spectral resolution measurements by quantum probes, Phys. Rev. Lett. **122,** 060503 (2019).

[5] T. Gefen, A. Rotem, and A. Retzker, Overcoming resolution limits with quantum sensing, Nat. Commun. **10,** 4992 (2019).

[6] T. Staudacher, F. Shi, S. Pezzagna, J. Meijer, J. Du, C. A. Meriles, F. Reinhard, and J. Wrachtrup, Nuclear magnetic resonance spectroscopy on a (5-Nanometer)^3 sample volume, Science **339,** 561 (2013).

[7] H. J. Mamin, M. Kim, M. H. Sherwood, C. T. Rettner, K. Ohno, D. D. Awschalom, and D. Rugar, Nanoscale nuclear magnetic resonance with a nitrogen-vacancy spin sensor, Science **339,** 557 (2013).

[8] C. Müller, X. Kong, J.-M. Cai, K. Melentijevic, A. Stacey, M. Markham, D. Twitchen, J. Isoya, S. Pezzagna, J. Meijer, J. F. Du, M. B. Plenio, B. Naydenov, L. P. McGuinness, and F. Jelezko, Nuclear magnetic resonance spectroscopy with single spin sensitivity, Nat. Commun. **5,** 4703 (2014).

[9] A. Ajoy, U. Bissbort, M. D. Lukin, R. L. Walsworth, and P. Cappellaro, Atomic-Scale Nuclear Spin Imaging Using Quantum-Assisted Sensors in Diamond, Phys. Rev. X **5,** 011001 (2015).

[10] I. Lovchinsky, A. O. Sushkov, E. Urbach, N. P. de Leon, S. Choi, K. De Greve, R. Evans, R. Gertner, E. Bersin, C. Müller, L. McGuinness, F. Jelezko, R. L. Walsworth, H. Park, and M. D. Lukin, Nuclear magnetic resonance detection and spectroscopy of single proteins using quantum logic, Science **351,** 836 (2016).

[11] N. Aslam, M. Pfender, P. Neumann, R. Reuter, A. Zappe, F. F. de Oliveira, A. Denisenko, H. Sumiya, S. Onoda, J. Isoya, and J. Wrachtrup, Nanoscale nuclear magnetic resonance with chemical resolution, Science **357,** 67 (2017).

[12] D. B. Bucher, D. R. Glenn, H. Park, M. D. Lukin, and R. L. Walsworth, Hyperpolarization-Enhanced NMR Spectroscopy with Femtomole Sensitivity Using Quantum Defects in Diamond, Phys. Rev. X **10,** 021053 (2020).

[13] F. Shagieva, A. Zappe, D. Cohen, A. Denisenko, A. Retzker, and J. Wrachtrup, Lateral diffusion of phospholipids in artificial cell membranes measured by single shallow NV centers, arXiv:2105.07712.

[14] R. D. Allert, F. Bruckmaier, N. R. Neuling, F. A. Freire-Moschovitis, K. S. Liu, C. Schrepel, P. Schätzle, P. Knittel, M. Hermans, and D. B. Bucher, Microfluidic quantum sensing platform for lab-on-a-chip applications, Lab Chip **22,** 4831 (2022).

[15] F. A. Freire-Moschovitis, R. Rizzato, A. Pershin, M. R. Schepp, R. D. Allert, L. M. Todenhagen, M. S. Brandt, A. Gali, and D. B. Bucher, The role of electrolytes in the relaxation of near-surface spin defects in diamond, ACS Nano **17,** 10474 (2023).

[16] L. Nie, A. C. Nusantara, V. G. Damle, R. Sharmin, E. P. P. Evans, S. R. Hemelaar, K. J. van der Laan, R. Li, F. P. P. Martinez, T. Vedelaar, M. Chipaux, and R. Schirhagl, Quantum monitoring of cellular metabolic activities in single mitochondria, Sci. Adv. **7,** eabf0573 (2021).

[17] A. Laraoui, F. Dolde, C. Burk, F. Reinhard, J. Wrachtrup, and C. A. Meriles, High-resolution correlation spectroscopy of ^{13}C spins near a nitrogen-vacancy centre in diamond, Nat. Commun. **4,** 1651 (2013).

[18] C. L. Degen, M. Poggio, H. J. Mamin, and D. Rugar, Role of spin noise in the detection of nanoscale ensembles of nuclear spins, Phys. Rev. Lett. **99,** 250601 (2007).

[19] F. Reinhard, F. Shi, N. Zhao, F. Rempp, B. Naydenov, J. Meijer, L. T. Hall, L. Hollenberg, J. Du, R.-B. Liu, and J. Wrachtrup, Tuning a Spin bath through the quantum-classical transition, Phys. Rev. Lett. **108,** 200402 (2012).

[20] B. E. Herzog, D. Cadeddu, F. Xue, P. Peddibhotla, and M. Poggio, Boundary between the thermal and statistical polarization regimes in a nuclear spin ensemble, Appl. Phys. Lett. **105,** 043112 (2014).

[21] L. M. Pham, S. J. DeVience, F. Casola, I. Lovchinsky, A. O. Sushkov, E. Bersin, J. Lee, E. Urbach, P. Cappellaro, H. Park, A. Yacoby, M. Lukin, and R. L. Walsworth, NMR technique for determining the depth of shallow nitrogen-vacancy centers in diamond, Phys. Rev. B **93,** 045425 (2016).

[22] D. Cohen, R. Nigmatullin, O. Kenneth, F. Jelezko, M. Khodas, and A. Retzker, Utilising NV based quantum sensing for velocimetry at the nanoscale, Sci. Rep. **10,** 5298 (2020).

[23] S. Oviedo-Casado, A. Rotem, R. Nigmatullin, J. Prior, and A. Retzker, Correlated noise in Brownian motion allows for super resolution, Sci. Rep. **10,** 19691 (2020).

[24] D. Cohen, T. Gefen, L. Ortiz, and A. Retzker, Achieving the ultimate precision limit with a weakly interacting quantum probe, npj Quantum Inf. **6,** 83 (2020).

[25] N. Staudenmaier, A. Vijayakumar-Sreeja, S. Oviedo-Casado, G. Genov, D. Cohen, D. Dulog, T. Unden, N. Striegler, A. Marshall, J. Scheuer, C. Findler, J. Lang, I. Schwartz, P. Neumann, A. Retzker, and F. Jelezko, Power-law scaling of correlations in statistically polarised nano-NMR, npj Quantum Inf. **8,** 120 (2022).

[26] L. Viola, E. Knill, and S. Lloyd, Dynamical decoupling of open quantum systems, Phys. Rev. Lett. **82,** 2417 (1999).

[27] L. Cywiński, R. M. Lutchyn, C. P. Nave, and S. Das Sarma, How to enhance dephasing time in superconducting qubits, Phys. Rev. B **77,** 174509 (2008).

[28] C. A. Ryan, J. S. Hodges, and D. G. Cory, Robust decoupling techniques to extend quantum coherence in diamond, Phys. Rev. Lett. **105,** 200402 (2010).

[29] A. M. Souza, G. A. Álvarez, and D. Suter, Robust dynamical decoupling for quantum computing and quantum memory, Phys. Rev. Lett. **106,** 240501 (2011).

[30] J. Casanova, Z.-Y. Wang, J. F. Haase, and M. B. Plenio, Robust dynamical decoupling sequences for individual-nuclear-spin addressing, Phys. Rev. A **92,** 042304 (2015).

[31] D. Suter and G. A. Álvarez, Colloquium: Protecting quantum information against environmental noise, Rev. Mod. Phys. **88,** 041001 (2016).

[32] G. T. Genov, D. Schraft, N. V. Vitanov, and T. Halfmann, Arbitrarily accurate pulse sequences for robust dynamical decoupling, Phys. Rev. Lett. **118,** 133202 (2017).

[33] See Supplemental Material at http://link.aps.org/supplemental/10.1103/PhysRevLett.131.150801 for a

detailed description of the Qdyne protocol procedure, setup and samples details, measurements optimization specifics, post-processing analysis approach, and detailed theoretical derivations, which includes Refs. [34–42].

[34] J. M. Binder, A. Stark, N. Tomek, J. Scheuer, F. Frank, K. D. Jahnke, C. Müller, S. Schmitt, M. H. Metsch, T. Unden, T. Gehring, A. Huck, U. L. Andersen, L. J. Rogers, and F. Jelezko, Qudi: A modular python suite for experiment control and data processing, SoftwareX **6**, 85 (2017).

[35] C. Osterkamp, M. Mangold, J. Lang, P. Balasubramanian, T. Teraji, B. Naydenov, and F. Jelezko, Engineering preferentially-aligned nitrogen-vacancy centre ensembles in CVD grown diamond, Sci. Rep. **9**, 5786 (2019).

[36] C. Findler, J. Lang, C. Osterkamp, M. Nesládek, and F. Jelezko, Indirect overgrowth as a synthesis route for superior diamond nano sensors, Sci. Rep. **10**, 22404 (2020).

[37] J. Lang, S. Häußler, J. Fuhrmann, R. Waltrich, S. Laddha, J. Scharpf, A. Kubanek, B. Naydenov, and F. Jelezko, Long optical coherence times of shallow-implanted, negatively charged silicon vacancy centers in diamond, Appl. Phys. Lett. **116**, 064001 (2020).

[38] S. C. Schmitt, Nanoscale magnetic spectroscopy with colour centres in diamond, Ulm University, 2020, https://oparu.uni-ulm.de/xmlui/handle/123456789/38675.

[39] J. Meinel, V. Vorobyov, B. Yavkin, D. Dasari, H. Sumiya, S. Onoda, J. Isoya, and J. Wrachtrup, Heterodyne sensing of microwaves with a quantum sensor, Nat. Commun. **12**, 2737 (2021).

[40] N. Staudenmaier, S. Schmitt, L. P. McGuinness, and F. Jelezko, Phase-sensitive quantum spectroscopy with high-frequency resolution, Phys. Rev. A **104**, L020602 (2021).

[41] D. Cohen, R. Nigmatullin, M. Eldar, and A. Retzker, Confined Nano-NMR Spectroscopy Using NV Centers, Adv. Quantum Technol. **3**, 2000019 (2020).

[42] A. Charnes, E. L. Frome, and P. L. Yu, The equivalence of generalized least squares and maximum likelihood estimates in the exponential family, J. Am. Stat. Assoc. **71**, 169 (1976).

[43] W. K. Wootters, Statistical distance and Hilbert space, Phys. Rev. D **23**, 357 (1981).

[44] S. L. Braunstein and C. M. Caves, Statistical distance and the geometry of quantum states, Phys. Rev. Lett. **72**, 3439 (1994).

[45] E. Abbe, Beiträge zur Theorie des Mikroskops und der mikroskopischen Wahrnehmung, Arch. Mikrosc. Anat. **9**, 413 (1873).

[46] F. Lord Rayleigh, XXXI. Investigations in optics, with special reference to the spectroscope, London, Edinburgh, Dublin Philos. Mag. J. Sci. **8**, 261 (1879).

[47] A. W. Jones, J. Bland-Hawthorn, and P. L. Shopbell, *Towards a General Definition for Spectroscopic Resolution*, edited by R. A. Shaw, H. E. Payne, and J. J. E. Hayes, Astronomical Society of the Pacific Conference Series Vol. 77 (1995), pp. 503–506.

[48] F. M. Dekking, C. Kraaikamp, H. P. Lopuhaä, and L. E. Meester, *A Modern Introduction to Probability and Statistics* (Springer, London, 2005).

[49] G. L. Bretthorst, *Bayesian Spectrum Analysis and Parameter Estimation* (Springer-Verlag, Berlin, 1988).

[50] V. Anh, Nonlinear least squares and maximum likelihood estimation of a heteroscedastic regression model, Stoch. Proc. Appl. **29**, 317 (1988).

[51] S. Schmitt, T. Gefen, D. Louzon, C. Osterkamp, N. Staudenmaier, J. Lang, M. Markham, A. Retzker, L. P. McGuinness, and F. Jelezko, Optimal frequency measurements with quantum probes, npj Quantum Inf. **7**, 55 (2021).

[52] J. Hadden, J. Harrison, A. C. Stanley-Clarke, L. Marseglia, Y.-L. Ho, B. Patton, J. L. O'Brien, and J. Rarity, Strongly enhanced photon collection from diamond defect centers under microfabricated integrated solid immersion lenses, Appl. Phys. Lett. **97**, 241901 (2010).

[53] P. Siyushev, F. Kaiser, V. Jacques, I. Gerhardt, S. Bischof, H. Fedder, J. Dodson, M. Markham, D. Twitchen, F. Jelezko *et al.*, Monolithic diamond optics for single photon detection, Appl. Phys. Lett. **97**, 241902 (2010).

[54] L. Robledo, L. Childress, H. Bernien, B. Hensen, P. F. Alkemade, and R. Hanson, High-fidelity projective read-out of a solid-state spin quantum register, Nature (London) **477**, 574 (2011).

[55] S. A. Momenzadeh, R. J. Stöhr, F. F. de Oliveira, A. Brunner, A. Denisenko, S. Yang, F. Reinhard, and J. Wrachtrup, Nanoengineered diamond waveguide as a robust bright platform for nanomagnetometry using shallow nitrogen vacancy centers, Nano Lett. **15**, 165 (2015).

[56] N. Aharon, A. Rotem, L. P. McGuinness, F. Jelezko, A. Retzker, and Z. Ringel, NV center based nano-NMR enhanced by deep learning, Sci. Rep. **9**, 17802 (2019).